applied sciences

MDPI

Article

Dispersion-Managed Tm-Ho Co-Doped Ultrashort Pulse Fiber Laser Using Single-Walled Carbon Nanotube and Spectral Filter

Keisuke Fukazawa [1], Ying Zhou [2], Shotaro Kitajima [1], Takeshi Saito [2], Youichi Sakakibara [2] and Norihiko Nishizawa [1,*]

[1] Department of Electronics, Nagoya University, Nagoya 464-8603, Japan
[2] National Institute of Advanced Industrial Science and Technology (AIST), Tsukuba 305-8568, Japan
* Correspondence: nishizawa@nuee.nagoya-u.ac.jp; Tel.: +81-52-789-3164

Featured Application: Biomedical imaging, Environmental spectroscopy, LIDAR, Medicine, and Laser processing.

Abstract: In this paper, we have demonstrated a dispersion-managed, high-power, Tm-Ho co-doped ultrashort pulse fiber laser using a single walled carbon nanotube (SWNT) dispersed in polyimide film. An in-line type spectral filter was developed to control the output pulse spectra. Two SWNT films with different modulation depths were examined as a mode-locker. Normal dispersion fiber was used in the fiber laser oscillator, and dependence on net cavity dispersion was investigated. Passive mode-locking was achieved in a wide dispersion range, from −0.319 to +0.101 ps^2. Stable soliton mode-locking operation and dissipative soliton mode-locking operations were observed. The pumping efficiency was ~3 times higher than that in a Tm-doped fiber laser with a similar configuration. The developed fiber laser showed self-start and stable operations, and this laser is useful for practical applications.

Keywords: fiber laser; ultrashort pulse; carbon nanotube

Citation: Fukazawa, K.; Zhou, Y.; Kitajima, S.; Saito, T.; Sakakibara, Y.; Nishizawa, N. Dispersion-Managed Tm-Ho Co-Doped Ultrashort Pulse Fiber Laser Using Single-Walled Carbon Nanotube and Spectral Filter. *Appl. Sci.* **2022**, *12*, 12369. https://doi.org/10.3390/app122312369

Academic Editor: Maria Michalska

Received: 7 November 2022
Accepted: 30 November 2022
Published: 2 December 2022

1. Introduction

The wavelength range around 2 μm is important for environmental spectroscopy, laser processing, biomedical imaging and medicine, laser imaging detection and ranging (LIDAR), etc. Thulium (Tm)-doped and thulium–holmium (Tm-Ho) co-doped fiber lasers are useful and promising laser sources at this wavelength range. Passively mode-locked ultrashort pulse fiber lasers have been demonstrated, using nonlinear polarization rotation (NPR) and a semiconductor saturable absorber mirror (SESAM) [1–5]. Since there are water vapor absorptions in this wavelength range, an all-fiber configuration is preferred to realize stable operation. Using nano-carbon materials, an all-fiber type ultrashort pulse fiber laser can easily be demonstrated.

The first demonstration of a Tm-doped fiber laser using a single walled carbon nanotube (SWNT) film was reported in 2008 [6]. Then, a dispersion management and wavelength tuning operation were reported by some groups [7–11]. Passively mode-locked ultrashort pulse Tm-doped fiber lasers using graphene devices in a similar manner have also been demonstrated [12–14].

In our previous work, we demonstrated that ultrashort Tm-doped fiber laser using SWNT dispersed in polyimide film [15]. SWNTs with an almost constant diameter of 1.6 nm were synthesized with the enhanced direct injection pyrolytic synthesis (e-DIPs) method, and thin polyimide film devices dispersed with SWNT were developed as the saturable absorber [16]. Stable soliton mode-locking, and high-power dissipative soliton mode-locking operation were achieved successfully.

One of the problems with the Tm-doped fiber laser is its low pumping efficiency. In our previous work using the Tm-doped fiber, the pumping efficiency from the pump laser to

fiber laser output was ~5%, and this requires improvement. The Tm-Ho co-doped fiber has wide-gain bandwidth and, thanks to the co-doping, high pumping efficiency is expected. So far, although there have been a few reports about a Tm-Ho co-doped fiber laser, power scaling, ultrashort pulse generation, and wavelength control are still desired [5,17–19].

In this work, we demonstrated a dispersion-manage, Tm-Ho co-doped ultrashort pulse fiber laser using SWNT polyimide film. In terms of its applications for biomedical imaging, control of the oscillation wavelength is required in order to achieve high gain in the following Tm-doped fiber amplifier [20]. In this work, an in-line tunable spectral filter was developed and applied for spectral control. The spectral filter is effective in suppressing the accompanying sidebands in a mode-locked pulse. It is also effective in achieving stable passive mode-locking. Two SWNT polyimide films with different absorption and modulation depths were examined as the mode-locker. The net cavity dispersion was varied from negative to positive, and the characteristics of output pulses were precisely investigated.

2. Experimental Method and Results

Figure 1 shows the configuration of the developed Tm-Ho co-doped ultrashort pulse fiber laser. A 1.4 m piece of Tm-Ho co-doped fiber (THDF) (TH-1100, Neufern, East Granby, CT, USA) was used as the gain fiber. The output of a single mode laser diode (TH1550, Thorlabs, Newton, MA, USA) was amplified with a double clad Erbium (Er)-Ytterbium (Yb) co-doped fiber amplifier (FA-33, PriTel, Naperville, IL, USA), and introduced into the THDF through a wavelength division multiplexed (WDM) coupler. As a mode-locker, we used polyimide film dispersed with SWNT [15]. SWNTs with an almost constant diameter of around 1.6 nm were selectively synthesized by the e-DIPS method [16]. The thicknesses of the films were 35–45 μm. They showed a strong absorption peak around 1.9 μm. In this work, we used two kinds of polyimide films, film A and film B, with different magnitudes of absorption. The modulation depths were 12.3% and 20.5% for films A and B, respectively [15]. The characteristics of the two films are summarized in Table 1.

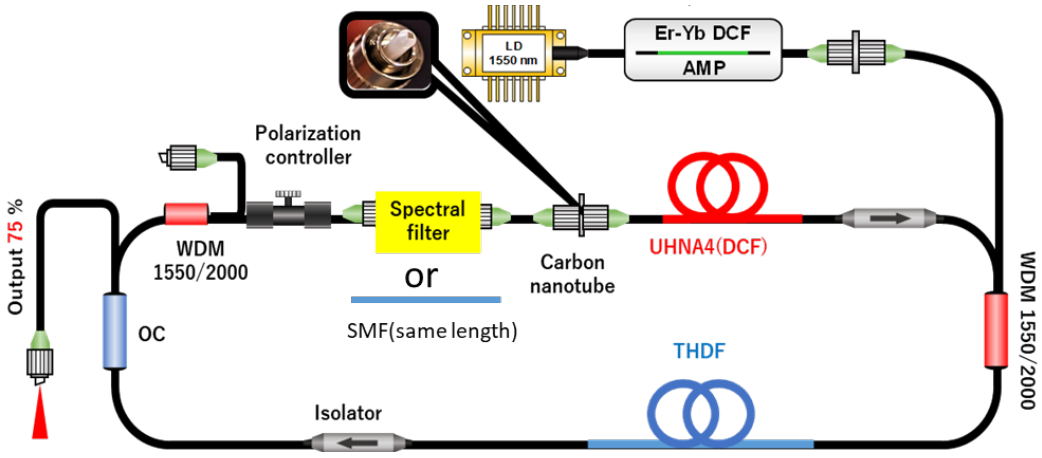

Figure 1. Configuration of Tm-Ho co-doped ultrashort pulse fiber laser using SWNT and in-line spectral filter.

Table 1. Characteristics of film A and film B [15].

	Thickness (μm)	Density of SWNT (wt%)	Modulation Depth (%)	Non-Saturable Absorption Ratio (%)	Saturation Power Fluence (MW/cm^2)
Film A	37–47	0.05	12.3	27.4	710
Film B	40–45	~0.08	20.5	34.4	620

The fiber laser cavity consisted of single mode fiber devices. Two optical isolators were used to realize the one way operation and to protect the SWNT polyimide film. A 75:25 coupler was used as the output coupler. An additional WDM coupler was used to remove the residual pump beam.

In order to realize the oscillation wavelength control without any spatial device, we developed an in-line wavelength tunable spectral filter. Figure 2 shows the configuration of the wavelength tunable spectral filter. It consisted of two polarizers, polarization maintaining fibers (PMFs), and single mode fiber (SMF) with a polarization controller (PC). The configuration is similar to that developed for a Yb-doped fiber laser in [21]. In this work, we applied a stress-applying type PC to realize the tunable operation. The FC/APC connectors were spliced at the ends of the filter, and easily inserted into the fiber laser cavity. An additional PC was used to control the optical loss at the first polarizer in the spectral filter.

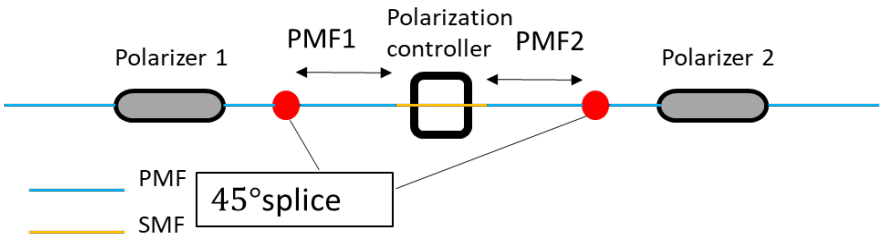

Figure 2. Configuration of wavelength tunable spectral filter based on birefringent fibers.

Polarizer 1 was spliced with PMF1, which was inclined by 45 degrees. For the output port, polarizer 2 was spliced with PMF2 which was also inclined by 45 degrees. A SMF with PC was inserted in between the PMF1 and PMF2. By the operation of the PC, we can demonstrate the bandwidth and wavelength tunable operation [21].

Figure 3 shows the wavelength dependence of the developed spectral filter. In this work, the lengths of PMF1, SMF, and PMF2 were 10 cm, 14.5 cm, and 7 cm, respectively. A wideband supercontinuum and optical spectrum analyzer were used for this measurement [22]. The transmission spectra were obtained by dividing the observed output spectra by the observed input spectra. The numerical results were analyzed using the Jones matrix. As shown in Figure 3a, the numerically obtained transmission spectra showed similar periodical behavior to the experimentally observed ones. The numerical and experimental transmission bandwidths were 29.5 nm and 23 nm, respectively. It was considered that the discrepancy between experimental and numerical spectra was mainly caused by the variation of parameters in the fiber devices. In the experiment, when the magnitude of applied stress was controlled in the PC, the transmission spectra were shifted continuously by the combination of polarization change and birefringence in PMFs, and the wavelength tunable operation was achieved, as shown in Figure 3b. A continuous wavelength tuning of 15 nm was observed. During the wavelength tuning operation, the peak–peak contrast changes as well, owing to the effect of birefringence and polarization control. The sharp dips were caused by the effect of water absorption in air.

In this work, in order to examine the dependence on net cavity dispersion, an ultrahigh numerical aperture fiber (UHNA4) which has strong normal dispersion property was used to vary the net cavity dispersion. The total dispersion was varied from negative to strong positive by changing the length of the UHNA4 between 0 and 4.8 m, and the mode-locking properties were examined. The corresponding repetition rate was 36.3–19.4 MHz. In order to examine the role and effectiveness of the spectral filter, a SMF with the same length of the birefringent spectral filter was used to keep the magnitude of the net cavity dispersion and repetition rate.

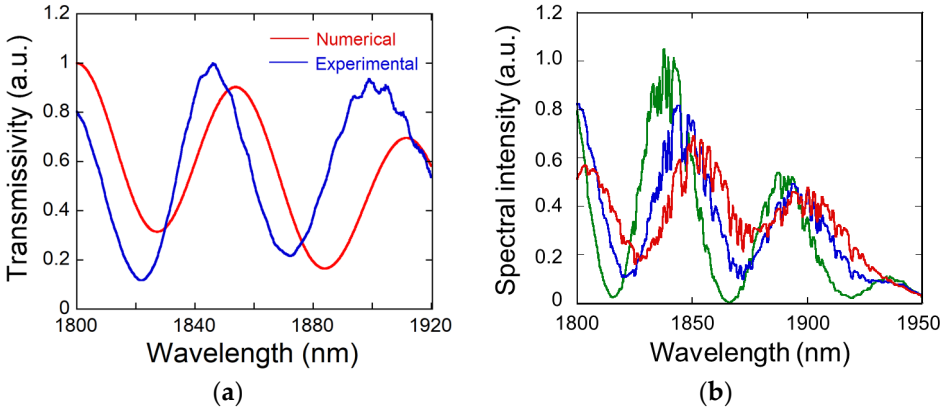

Figure 3. Wavelength dependence of developed tunable filter, (**a**) comparison of numerical and experimental transmission spectra, and (**b**) variation of transmitted spectra during the wavelength tuning operation.

Figure 4a,b show the variation of optical spectra when film A was used. The magnitude of net cavity dispersion was changed from -0.319 ps^2 to 0.1010 ps^2. Mode-locking was obtained in these wide dispersion conditions without the spectral filter. When the developed filter was applied, a wavelength tuning operation was achieved in an anomalous dispersion region. Since there was a limitation of bandwidth by the spectral filter, mode-locking was not obtained around the zero-dispersion region.

Figure 4c,d show the variation of optical spectra when film B was used. Here, the mode-locking operation was confirmed for net cavity dispersion from -0.319 ps^2 to 0.1010 ps^2. Stable mode-locking was obtained in this wide dispersion range. Since the magnitude of absorption was larger in film B compared to film A, film B was useful to suppress the additional cw oscillation. A wavelength tunable operation was obtained in the anomalous dispersion region.

Compared with the previous work that used a Tm-doped fiber, the same output power was obtained with much lower pump power [15]. The estimated pumping efficiency was improved by ~3 times, compared to that of a Tm-doped fiber laser using the same SWNT film.

Next, we discuss the dependence on net-cavity dispersion.

2.1. Anomalous Dispersion Region

First, we focus on the anomalous dispersion region. When the net cavity dispersion D was between -0.319 and -0.0197 ps^2, stable soliton mode-locking was achieved. When the spectral filter was not used, sech^2 shaped pulse spectra with strong Kelly sidebands, which are characteristics of a soliton mode-locked pulse, were generated stably. Since the chromatic dispersion of SMF was large and negative at this wavelength range, the magnitudes of Kelly sidebands were large, compared to conventional Er and Yb-doped fiber lasers. The spectral width was increased as the net cavity dispersion was close to zero.

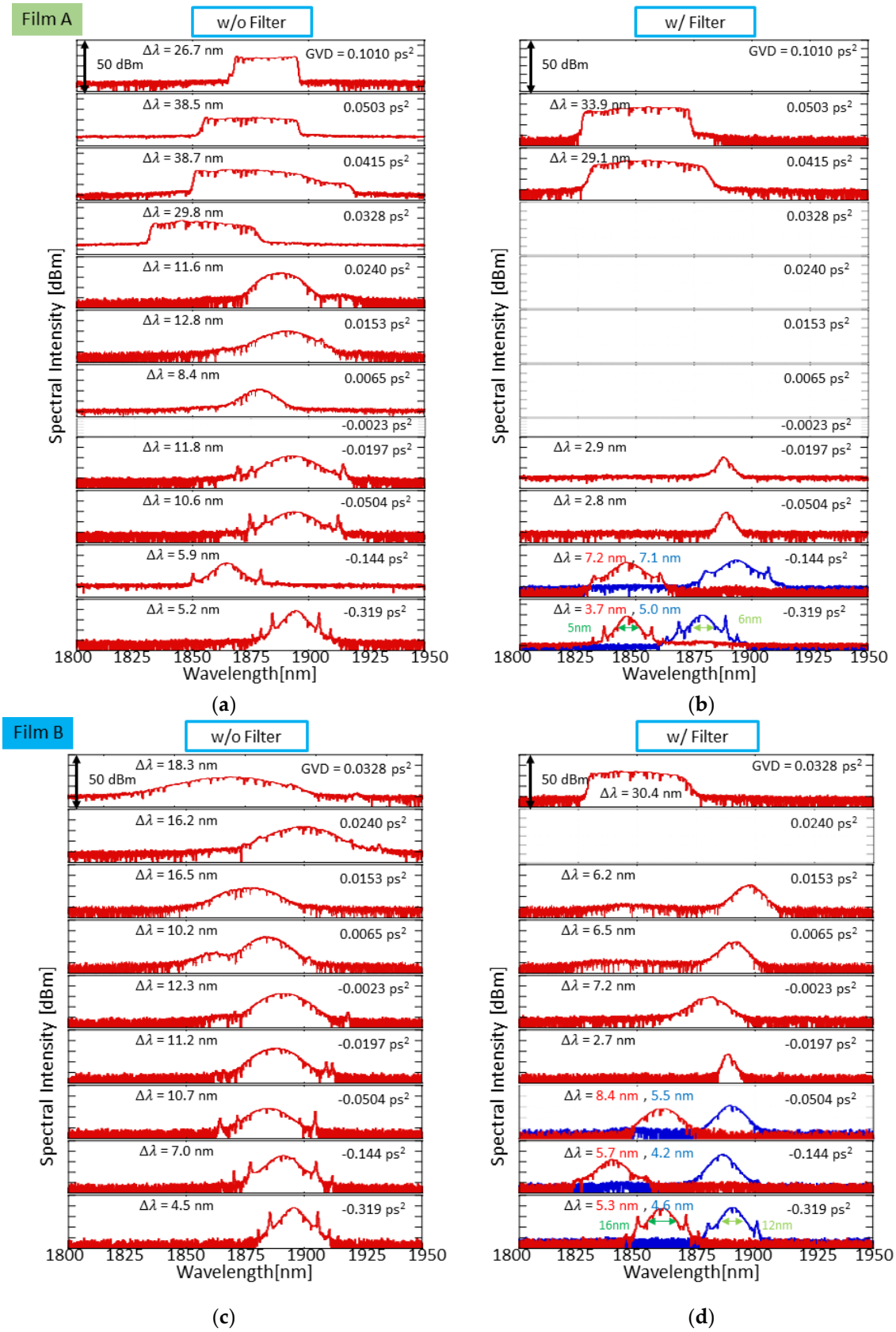

Figure 4. Variation of optical spectra at fiber laser output when net dispersion was varied. (**a**,**b**) film A was used and spectral filter was (**a**) not used and (**b**) used. (**c**,**d**) film B was used and spectral filter was (**c**) not used and (**d**) used.

When the spectral filter was used, passive mode-locking was achieved for the dispersion of −0.319 to −0.0197 ps^2. For D = −0.319 and −0.144 ps^2, sech^2 shaped pulses were obtained stably. Particularly when D = −0.144 ps^2, the properties of the spectral filter fitted the laser performance well. A sech^2 shaped pulse with 7.2 nm spectral width and suppressed Kelly sidebands were obtained stably. It is interesting to note that, as shown by the blue and red curves in Figure 4, there were conditions in which mode-locking was obtained at two different center wavelengths. When D = −0.319 ps^2, a continuous wavelength tuning operation was achieved by the control of the PC in the spectral filter. As shown by the green arrows in Figure 4b,d, the magnitudes of the tuning range were 5 to 16 nm. In addition, the switching of the center wavelength of the mode-locked pulse, which is shown in the blue and red curves, was demonstrated by the operation of the PC before the spectral filter. The shortest center wavelength was 1840 nm, which is useful to generate a high power soliton pulse at the 2.0 µm range using a Tm-doped fiber amplifier [20]. For D = −0.05 and −0.0197 ps^2, narrow spectra of 2.8–2.9 nm were observed. It was considered that these narrow spectra were due to the bandwidth limit of the spectral filter.

Figure 5 show the representative characteristics of output pulses for the net anomalous dispersion region when the spectral filter was not used. Here, the net cavity dispersion D = −0.144 ps^2. A sech^2 shaped pulse with intense Kelly sidebands is shown in Figure 5a. Here, the spectral width was 7.1 nm at full-width half-maximum (FWHM). A clean autocorrelation trace without pedestal component is shown in Figure 5b. The temporal width was 999 fs, and the corresponding pulse width was 648 fs under the assumption of the sech^2 shaped pulse. The estimated time bandwidth product was 0.387, which was close to that of the Fourier transform limited sech^2 shaped pulse. In the radio frequency (RF) domain, clean RF spectra were observed. For the fundamental frequency shown in Figure 5d, the observed signal-to-noise ratio (SNR) was about 70 dB, and a low noise property was confirmed. In the RF spectra in the wide range shown in Figure 5e, clean RF spectra with almost constant intensity were observed up to 2 GHz, and stable mode-locking was confirmed.

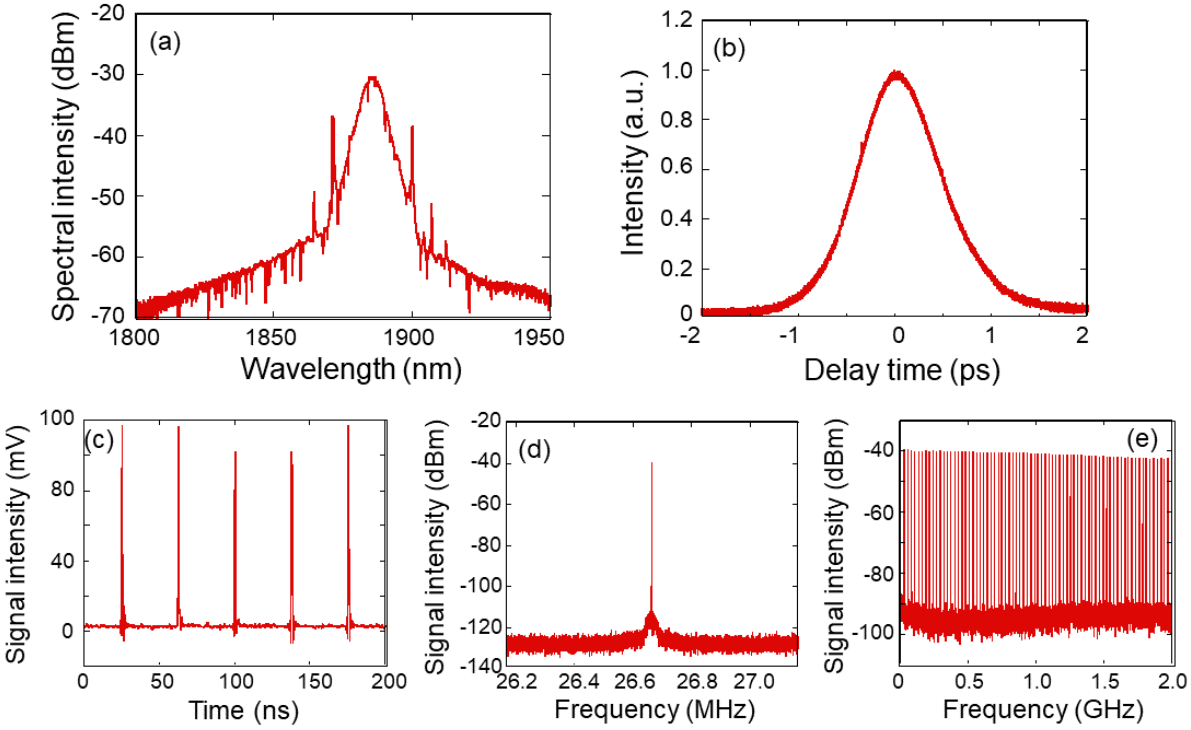

Figure 5. Characteristics of output pulses when D = −0.144 ps^2 and spectral filter was not used, (**a**) optical spectra, (**b**) autocorrelation trace, (**c**) pulse train, (**d**,**e**) RF spectra of (**d**) fundamental frequency and (**e**) wide range.

Figure 6 shows the characteristics of output pulses when $D = -0.144$ ps^2 and the spectral filter was used. Here the magnitudes of Kelly sidebands were suppressed well, and cleaner optical spectra are shown in Figure 6a. The observed spectral width was 5.8 nm at FWHM. The temporal width of the autocorrelation trace is 1016 fs in Figure 6b, and the corresponding pulse width is 659 fs, under the assumption of a sech^2 shaped pulse. The time bandwidth product was 0.319. In the RF domain, the observed SNR was 70 dB in Figure 6d, and stable mode-locking is confirmed in Figure 6e.

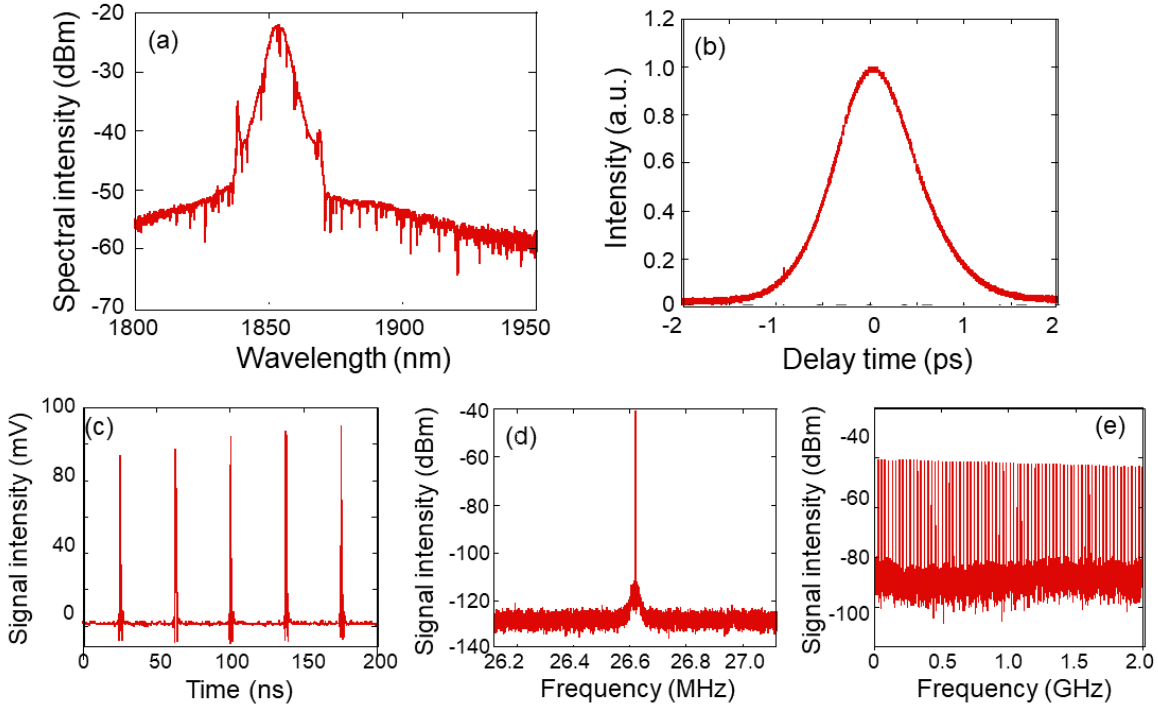

Figure 6. Characteristics of output pulses when $D = -0.144$ ps^2 and spectral filter was used, (**a**) optical spectra, (**b**) autocorrelation trace, (**c**) pulse train, (**d**,**e**) RF spectra of (**d**) fundamental frequency and (**e**) wide range.

2.2. Around Zero Dispersion Region

Next, we discuss the dispersion region close to zero, where the net cavity dispersion D was from -0.0023 to $+0.0328$ ps^2. When film A was used and the spectral filter was not used, passive mode-locking was obtained within the $+0.0065$ to $+0.0328$ ps^2 range. In the range from $+0.0065$ to 0.024 ps^2, smooth and mono-peak spectra without sidebands were observed. The spectral width was 8.4 to 11.6 nm. When $D = +0.0328$ ps^2, a dissipative soliton pulse with steep edges was observed. The spectral width was as wide as 29.8 nm. When $D = -0.0023$ ps^2, stable mode-locking was not obtained.

Figure 7 shows the characteristics of output pulses when $D = +0.0153$ ps^2. Mono-peak spectra without Kelly sidebands were observed stably, as shown in Figure 7a. The sharp spectral peaks were caused by the water vapor absorption. For the auto-correlation trace, the temporal width was 882 fs, as shown in Figure 7b, and the corresponding pulse width was 570 fs, under the assumption of a sech^2 shaped pulse. In the RF spectra, the SNR was more than 70 dB, as shown in Figure 7d, and good mode-locking was obtained.

When the spectral filter and film A were used, as shown in Figure 4, stable mode-locking was not obtained in this dispersion condition. Here, we discuss the physical background for these results. Around the zero-dispersion region, stretched pulse mode-locking is the dominant mode-locking operation. In this operation, the spectral width of a mode-locked pulse becomes wider through the accompanying nonlinear effect. In order to sustain the broad pulse spectra, the wider bandwidth of a spectral filter is required for the generation of such pulses. In addition, previous studies have shown that a large

modulation depth is required to obtain a stretched pulse mode-locking operation [23]. Since the modulation depth of film A was smaller than that of film B, it was difficult to obtain passive mode-locking when film A and the spectral filter were used.

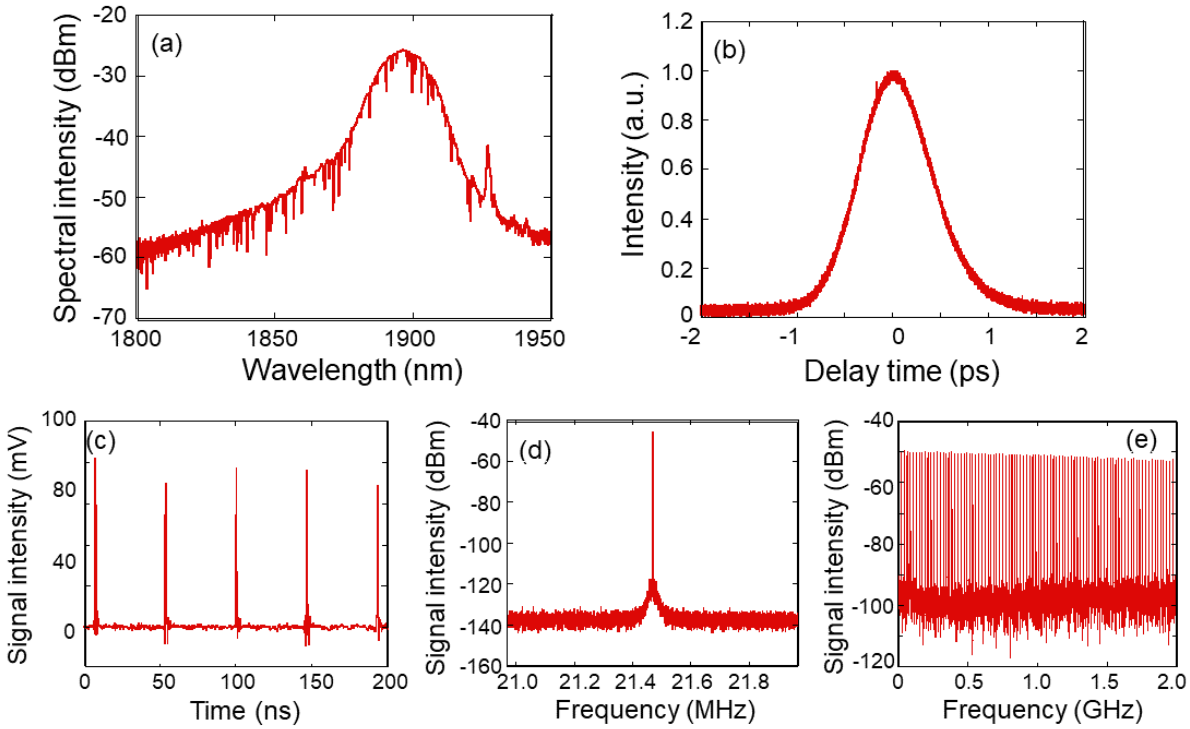

Figure 7. Characteristics of output pulses when D = +0.0153 ps^2 and spectral filter was not used, (**a**) optical spectra, (**b**) autocorrelation trace, (**c**) pulse train, (**d**,**e**) RF spectra of (**d**) fundamental frequency and (**e**) wide range.

Next, we focus on the condition in which film B was used and D ranged from −0.0023 to +0.0328 ps^2. Thanks to the large modulation depth in film B, stable mode-locking was achieved for these wider conditions, regardless of the usage of the spectral filter, as shown in Figure 4. The output power was lower than that obtained with film A.

2.3. Normal Dispersion Region

Next, we discuss the characteristics in the large normal dispersion region, where the net cavity dispersion D ranged from +0.0415 to +0.1010 ps^2. When film A was used and the spectral filter was not used, dissipative soliton mode-locking was obtained, and pulse spectra with steep edges were observed, as shown in Figure 4a. The spectral width was at its widest in this condition. The operation was a little unstable for D = +0.0415 and +0.0503 ps^2. When the spectral filter was used, stable mode-locking was obtained in these two dispersion conditions. The highest output power of 75.7 mW was obtained with the spectral filter when D = +0.0503 ps^2. When film B was used, passive mode-locking was not obtained in this dispersion region.

Figure 8 shows the representative characteristics of output pulses for this large normal dispersion condition. Here, the net cavity dispersion was +0.0503 ps^2. When the filter was not used, the spectral width was 24.4 nm, and a long-term stable operation was not obtained.

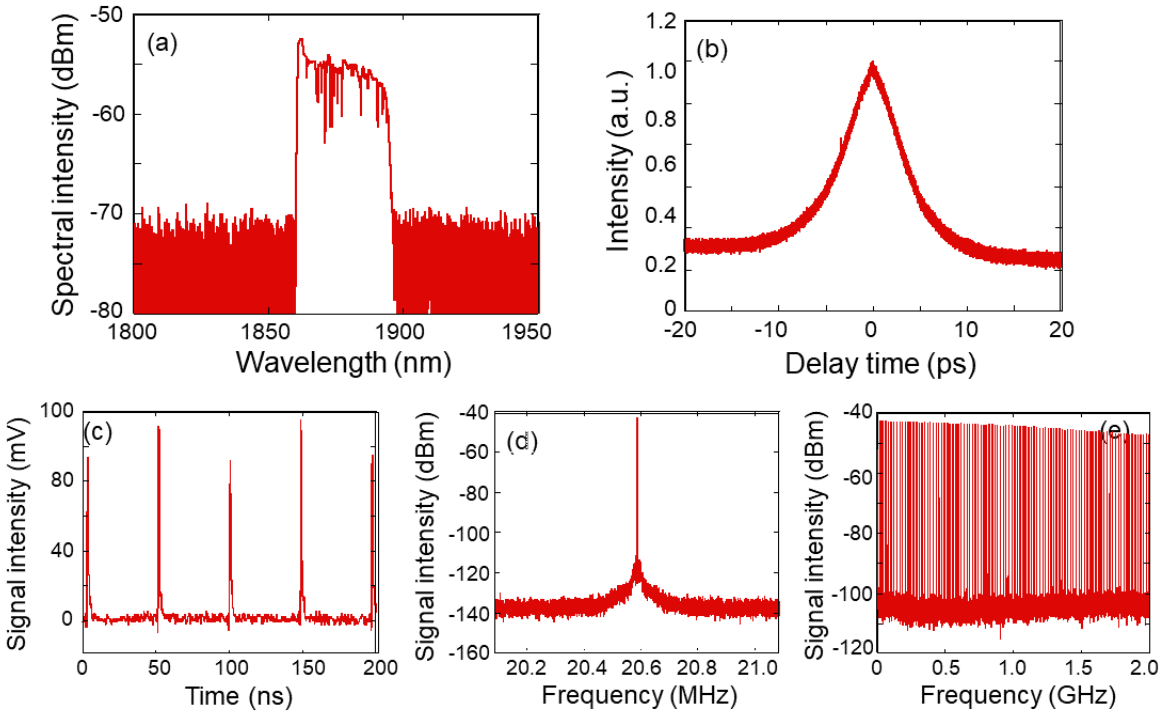

Figure 8. Characteristics of output pulses when D = +0.0503 ps^2 and spectral filter was not used, (**a**) optical spectra, (**b**) autocorrelation trace, (**c**) pulse train, (**d**,**e**) RF spectra of (**d**) fundamental frequency and (**e**) wide range.

Figure 9 shows the characteristics of output pulses when the spectral filter was used. In this case, stable mode-locking was obtained, and the highest output power of ~80 mW was achieved. In the RF spectra, the SNR was about 80 dB, as shown in Figure 9d. The temporal width of the autocorrelation trace was 5.4 ps, as shown in Figure 9b, and the corresponding pulse width was 3.5 ps, under the assumption of a sech^2 shaped pulse. The spectral filter was effective in obtaining a stable mode-locking operation in this condition.

2.4. Overall Net Cavity Dispersion Dependence

Figure 10 shows the overall characteristics of the developed fiber laser output as a function of net cavity dispersion D. The green area shows the condition in which mode-locking was obtained only when the spectral filter was not used. The orange area shows the condition in which mode-locking was not obtained. Almost transform-limited short soliton pulses were obtained in the anomalous dispersion region for both film A and B. It is interesting to note that the output power was larger when the spectral filter was used. Around the zero-dispersion region, stable mode-locking was obtained when film B was used. In the normal dispersion region, dissipative soliton pulses with high output power and a broad spectral width were obtained. The highest output power, up to about 80 mW, was achieved in the strong normal dispersion region when the spectral filter was used. Mode-locking was not obtained for film B. The observed behaviors were similar to those shown in Figure 9 in [15] for a Tm-doped fiber laser. As mentioned before, the pumping efficiency was ~3 times larger for the Tm-Ho co-doped fiber laser, compared to that of a Tm-doped fiber laser, and an efficient operation was obtained.

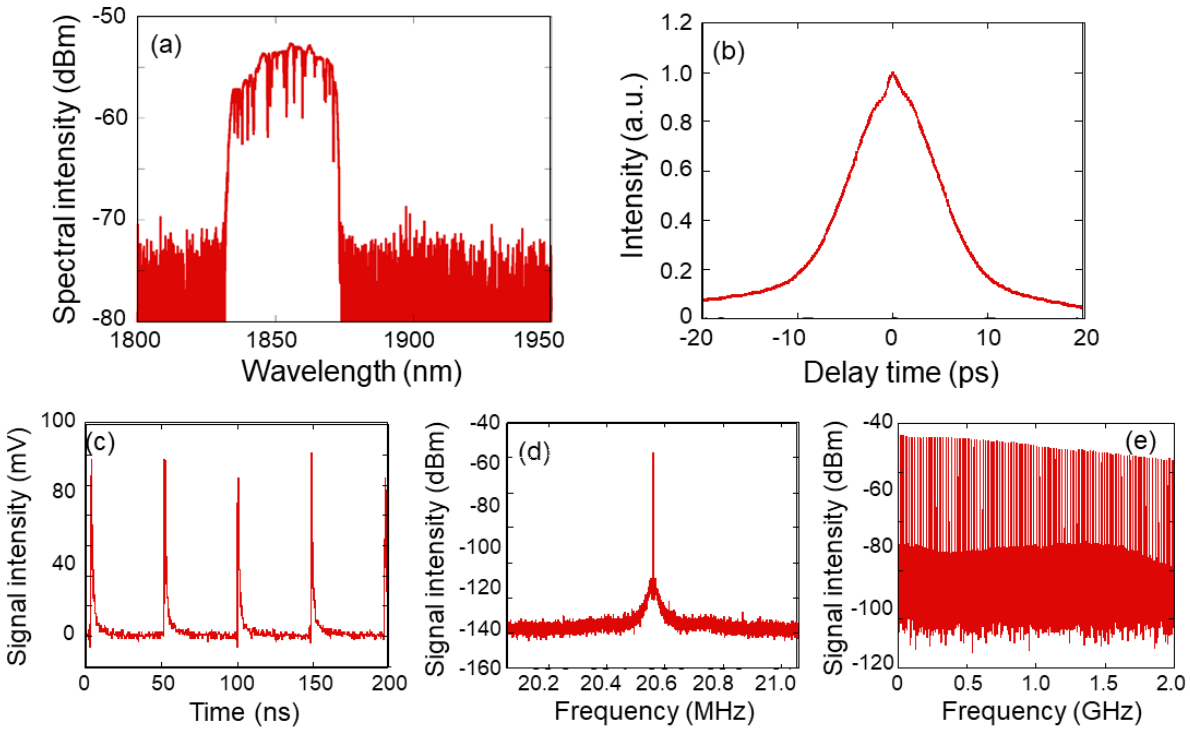

Figure 9. Characteristics of output pulses when D = +0.0503 ps^2 and spectral filter was used, (**a**) optical spectra, (**b**) autocorrelation trace, (**c**) pulse train, (**d**,**e**) RF spectra of (**d**) fundamental frequency and (**e**) wide range.

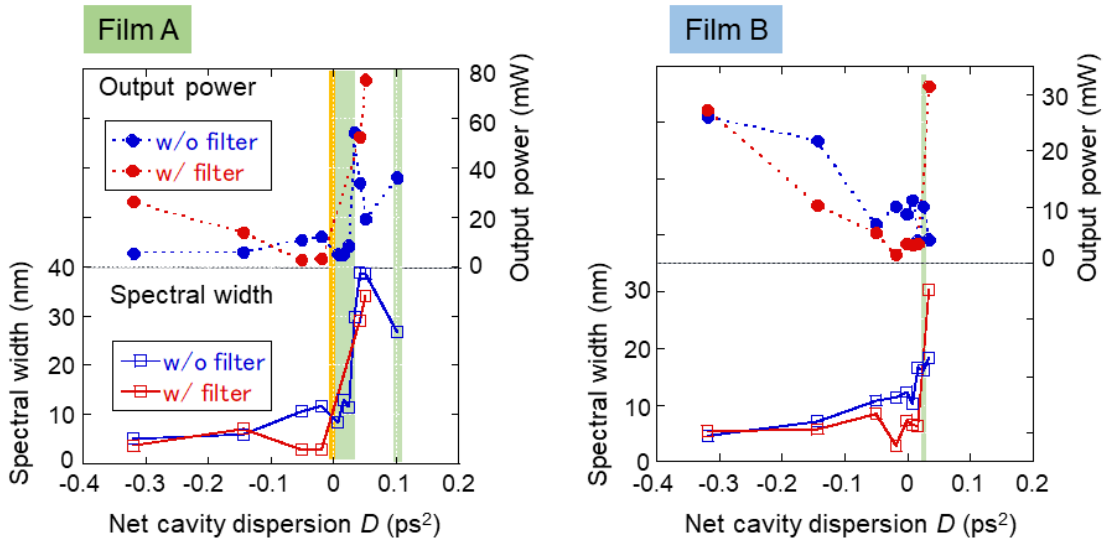

(**a**) (**b**)

Figure 10. Variation of characteristics of output pulses as a function of net cavity dispersion when (**a**) film A and (**b**) film B were used, respectively. Green areas show the region where mode-locking was obtained only when spectral filter was not used, and orange area shows the region where mode-locking was not obtained.

3. Conclusions

In this work, we demonstrated a dispersion-managed, passively mode-locked, ultrashort pulse, Tm-Ho co-doped fiber laser using SWNTs dispersed in polyimide film. An in-line type spectral filter was developed to control the oscillation spectra. The net

cavity dispersion was controlled using a normal dispersive fiber, and the characteristics of output pulses were investigated. Dependences on the spectral filter and SWNT films were, additionally, investigated.

Mode-locking was obtained in wide dispersion conditions, from −0.319 to +0.101 ps^2. In the anomalous dispersion region, almost transform-limited, short soliton pulses were obtained. The spectral filter was effective in suppressing Kelly sidebands and the wavelength tunable operation. Around the zero-dispersion region, stable mode-locking was obtained when film B with a larger modulation depth was used. For the normal dispersion region, high power, dissipative soliton pulses with a wide spectral width were obtained for film A. The maximum average power was 75.7 mW. The spectral filter was effective in achieving a high power, stable operation in the normal dispersion region.

A stable operation was observed experimentally, and it is expected that the developed Tm-Ho co-doped SWNT fiber laser will be useful for practical applications, such as biomedical imaging, spectroscopy, etc.

Author Contributions: Conceptualization, Y.S. and N.N.; methodology, Y.S. and N.N.; investigation, K.F., S.K. and N.N.; resources, Y.Z., Y.S., T.S. and N.N.; writing—original draft preparation, N.N.; writing—review and editing, N.N.; supervision, Y.S. and N.N.; project administration, Y.S. and N.N.; funding acquisition, N.N. All authors have read and agreed to the published version of the manuscript.

Funding: This work was supported by JSPS KAKENHI Grant Number 20H00350.

Data Availability Statement: Data underlying the results presented in this paper are not publicly available at this time but may be obtained from the authors upon reasonable request.

Conflicts of Interest: The authors declare no conflict of interest.

References

1. Nelson, L.E.; Ippen, E.P.; Haus, H.A. Broadly tunable sub-500 fs pulses from an additive-pulse mode-locked thulium-doped fiber ring laser. *Appl. Phys. Lett.* **1995**, *67*, 19–21. [CrossRef]
2. Engelbrecht, M.; Haxsen, F.; Ruehl, A.; Wandt, D.; Kracht, D. Ultrafast thulium-doped fiber-oscillator with pulse energy of 4.3 nJ. *Opt. Lett.* **2008**, *33*, 690–692. [CrossRef] [PubMed]
3. Haxsen, F.; Ruehl, A.; Engelbrecht, M.; Wandt, D.; Morgner, U.; Kracht, D. Stretched-pulse operation of a thulium-doped fiber laser. *Opt. Express* **2008**, *16*, 20471–20476. [CrossRef]
4. Tang, Y.; Chong, A.; Wise, F.W. Generation of 8 nJ pulses from a normal-dispersion thulium fiber laser. *Opt. Lett.* **2015**, *40*, 2361–2364. [CrossRef]
5. Gumenyuk, R.; Vartiainen, I.; Tuovinen, H.; Okhotnikov, O. Dissipative dispersion-managed soliton 2 um thulium/holmium fiber laser. *Opt. Lett.* **2011**, *36*, 609–611. [CrossRef]
6. Solodyankin, M.A.; Obraztsova, E.D.; Lobach, A.S.; Chernov, A.I.; Aausenev, A.V.; Konov, V.I.; Dianov, E.M. Mode-locked 1.93 um thulium fiber laser with a carbon nanotube absorber. *Opt. Lett.* **2008**, *33*, 1336–1338. [CrossRef] [PubMed]
7. Kivistö, S.; Hakulinen, T.; Kaskela, A.; Aitchison, B.; Brown, D.P.; Nasibulin, A.G.; Kauppinen, E.I.; Härkönen, A.; Okhotnikov, O.G. Carbon nanotube films for ultrafast broadband technology. *Opt. Express* **2009**, *17*, 2358–2363. [CrossRef]
8. Kieu, K.; Wise, F.W. Soliton Thulium-Doped Fiber Laser with Carbon Nanotube Saturable Absorber. *IEEE Photonics Technol. Lett.* **2009**, *21*, 128–130. [CrossRef]
9. Wang, Y.; Alam, S.-H.; Obraztsova, E.D.; Pozharov, A.S.; Set, S.Y.; Yamashita, S. Generation of stretched pulses and dissipative solitons at 2 μm from an all-fiber mode-locked laser using carbon nanotube saturable absorber. *Opt. Lett.* **2016**, *41*, 3864–3867. [CrossRef]
10. Wang, J.; Liang, X.; Hu, G.; Zheng, Z.; Lin, S.; Ouyang, D.; Wu, X.; Yan, P.; Ruan, S.; Sun, Z.; et al. 152 fs nanotube-mode-locked thulium-doped all-fiber laser. *Sci. Rep.* **2016**, *6*, 28885. [CrossRef]
11. Meng, Y.; Li, Y.; Xu, Y.; Wang, F. Carbon nanotube mode-locked thulium fiber laser with 200 nm tuning range. *Sci. Rep.* **2017**, *7*, 45109. [CrossRef]
12. Zhang, M.; Kelleher, E.J.R.; Torrisi, F.; Sun, Z.; Hasan, T.; Popa, D.; Wang, F.; Ferrari, A.C.; Popov, S.V.; Taylor, J.R. Tm-doped fiber laser made-locked by graphene-polymer composite. *Opt. Express* **2012**, *20*, 25077–25084. [CrossRef]
13. Sotor, J.; Bogusławski, J.; Martynkien, T.; Mergo, P.; Krajewska, A.; Przewłoka, A.; StrupiŃski, W.; SoboŃ, G. All-polarization-maintaining, stretched-pulse Tm-doped fiber laser, mode-locked by a graphene saturable absorber. *Opt. Lett.* **2017**, *42*, 1592–1595. [CrossRef] [PubMed]

14. Jeong, H.; Choi, S.Y.; Kim, M.H.; Rotermund, F.; Cha, Y.-H.; Jeong, D.-Y.; Lee, S.B.; Lee, K.; Yeom, D., II. All-fiber Tm-doped soliton laser with 6 nJ pulse energy based on evanescent field interaction with monolayer graphene saturable absorber. *Opt. Express* **2016**, *24*, 14152–14158. [CrossRef] [PubMed]
15. Watanabe, K.; Zhou, Y.; Sakakibara, Y.; Saito, Y.; Nishizawa, N. Dispersion-managed, high-power, Tm-doped ultrashort pulse fiber laser using single-wall-carbon-nanotub polyimide film. *OSA Contin.* **2021**, *4*, 137–148. [CrossRef]
16. Saito, T.; Ohshima, S.; Okazaki, T.; Ohmori, S.; Yumura, M.; Iijima, S. Selective diameter control of single-walled carbon nanotubes in the gas-phase synthesis. *J. Nanosci. Nanotechnol.* **2008**, *8*, 6153–6157. [CrossRef]
17. Jung, M.; Koo, J.; Park, J.; Song, Y.-W.; Jhon, Y.M.; Lee, K.; Lee, S.; Lee, J.H. Mode-locked pulse generation from an all-fiberized, Tm-Ho-codoped fiber laser incorporating a graphene oxide-deposited side-polished fiber. *Opt. Express* **2013**, *21*, 20062–20072. [CrossRef]
18. Kadel, R.; Washburn, B.R. Stretched-pulse and solitonic operation of an all-fiber thulium/holmium-doped fiber laser. *Appl. Opt.* **2015**, *54*, 746–750. [CrossRef]
19. Li, X.; Yu, X.; Sun, Z.; Yan, Z.; Sun, B.; Cheng, Y.; Yu, X.; Zhang, Y.; Wang, Q.J. High-power graphene mode-locked Tm/Ho co-doped fiber laser with evanescent field interaction. *Sci. Rep.* **2015**, *5*, 16624. [CrossRef]
20. Yamamoto, J.; Yamanaka, M.; Zhou, Y.; Saitoh, T.; Sakakibara, Y.; Nishizawa, N. Development of Supercontinuum Laser Source for 2 μm OCT with Tm-Ho co-doped Ultrashort Pulse Fiber Laser Using Single Wall Carbon Nanotube; STh5A.5. In Proceedings of the CLEO2021, A Virtual Conference, 9–14 May 2021.
21. Khanolkar, A.; Ge, X.; Chong, A. All-normal dispersion fiber laser with a bandwidth tunable fiber-based spectral filter. *Opt. Lett.* **2020**, *45*, 4555–4558. [CrossRef]
22. Nishizawa, N.; Takayanagi, J. Octave spanning high-quality supercontinuum generation in all-fiber system. *J. Opt. Soc. Am. B* **2007**, *24*, 1786–1792. [CrossRef]
23. Nishizawa, N.; Jin, L.; Kataura, H.; Sakakibara, Y. Dynamics of a Dispersion-Managed Passively Mode-Locked Er-Doped Fiber Laser Using Single Wall Carbon Nanotubes. *Photonics* **2015**, *2*, 808–824. [CrossRef]